A STUDY OF THE TRANSIENT FLOW FIELD AHEAD OF A SPHERE

WHICH HAS BEEN STRUCK BY A NORMAL SHOCK WAVE

By Richard W. Barnwell

NASA Langley Research Center
Langley Station, Hampton, Va.

Presented at the Tenth Midwestern Mechanics Conference

A STUDY OF THE TRANSIENT FLOW FIELD AHEAD OF A SPHERE

WHICH HAS BEEN STRUCK BY A NORMAL SHOCK WAVE

By Richard W. Barnwell

NASA Langley Research Center

ABSTRACT

When a normal shock wave moves into a still gas and strikes a blunt obstacle, the wave is diffracted, and a shock layer is formed on the upstream side of the obstacle. This shock layer adjusts with time until steady flow is established.

This paper presents numerical results for the normal-shock-wave—sphere interaction problem for perfect- and real-gas flow fields.

A finite difference method is used to solve the governing flow equations. The differencing technique which is employed is a modification to the technique which P. D. Lax developed for treating inviscid, unsteady one-dimensional-flow fields containing embedded shock waves.

Results are presented for the unsteady behavior of the shock detachment distance and the stagnation-point pressure. The cases which are treated cover wide ranges of the ratio of specific heats and the incident shock Mach number. The results show that the growth of the shock-layer thickness is much slower than the adjustment of the stagnation-point pressure to its steady value.

A STUDY OF THE TRANSIENT FLOW FIELD AHEAD OF A SPHERE

WHICH HAS BEEN STRUCK BY A NORMAL SHOCK WAVE

By Richard W. Barnwell

NASA Langley Research Center

INTRODUCTION

The transient flow which occurs when a normal shock wave moves into a still gas and strikes a sphere is to be investigated. This type of flow occurs in a shock tube which is being used as a supersonic wind tunnel during the period when steady flow about the model is being established. The flow field is assumed to be inviscid and adiabatic. Numerical results are presented for the time histories of the stagnation-point pressure and the shock-layer thickness along the stagnation streamline for a number of perfect-gas cases and two equilibrium-air cases.

The shock-wave—blunt-body interaction problem can be approximated by assuming that the body is placed in a still gas and accelerated instantaneously to supersonic speed. Cabannes (1), Bausset (2), and Miles, Mirels, and Wang (3) have used this assumption to obtain approximate analytical expressions for the time history of shock-layer thickness. Experimental results have been obtained for the transient behavior in the flow fields of various blunt bodies which have been washed by normal shock waves by Davies (4), Bryson and Gross (5), and Offenhartz and Weisblatt (6). Numerical results for diffraction of normal shock waves by a flat-nosed cylinder and a rectangular cylinder with its axis perpendicular to the flow have been obtained by Butler (7), who employs a numerical technique similar to the one which is used here.

L-5220

The Numerical Method

In the present investigation, numerical solutions are obtained to the initial value problem for the partial differential equations which govern unsteady inviscid gas flow and the boundary conditions for flow over a sphere. These solutions are calculated with a finite difference method which is based on a technique of first-order accuracy that P. D. Lax (8) developed for treating one-dimensional unsteady inviscid flow fields containing embedded shock waves. The virtue of the Lax technique is that the shock waves are not represented by apparent discontinuities in the flow property profiles, but rather by continuous profiles with steep gradients in the vicinity of the shocks.

The natural coordinate system for the present problem is a spherical polar system with its origin located at the center of the sphere and its axis directed along the stagnation streamline. The governing partial differential equations are used in conservation form. The equations which are employed at points away from the axis in the present work are:

Continuity:

$$\frac{\partial}{\partial t}(\rho r) + \frac{\partial}{\partial r}(\rho u r) + \frac{\partial}{\partial \theta}(\rho v) + \rho u + \rho v \cot \theta = 0 \tag{1}$$

Radial momentum:

$$\frac{\partial}{\partial t}(\rho u r) + \frac{\partial}{\partial r}\left[\left(p + \rho u^2\right)r\right] + \frac{\partial}{\partial \theta}(\rho u v) - p + \rho\left(u^2 - v^2\right) + \rho u v \cot \theta = 0 \tag{2}$$

Tangential momentum:

$$\frac{\partial}{\partial t}(\rho v r) + \frac{\partial}{\partial r}(\rho u v r) + \frac{\partial}{\partial \theta}\left(p + \rho v^2\right) + 2\rho u v + \rho v^2 \cot \theta = 0 \tag{3}$$

Energy:

$$\frac{\partial}{\partial t}(\rho E r) + \frac{\partial}{\partial r}(\rho u H r) + \frac{\partial}{\partial \theta}(\rho v H) + \rho u H + \rho v H \cot \theta = 0 \tag{4}$$

2

where

$$E = e + \frac{1}{2}\left(u^2 + v^2\right)$$

$$H = h + \frac{1}{2}\left(u^2 + v^2\right)$$

In these equations, r and θ are the standard polar coordinates, u and v are the velocity components in the r and θ directions, respectively, p, ρ, e, and h are the pressure, density, internal energy, and enthalpy of the gas, and t is the time.

Indeterminacies occur in equations (1) to (4) on the axis (θ = 0), where v vanishes and cot θ is infinite. These indeterminacies can be removed with the aid of l'Hospital's rule. For example, the continuity equation for θ = 0 is given by

$$\frac{\partial}{\partial t}(\rho r) + \frac{\partial}{\partial r}(\rho u r) + 2\frac{\partial}{\partial \theta}(\rho v) + \rho u = 0 \tag{5}$$

The general form of the governing equations is

$$\frac{\partial A_i}{\partial t} + \frac{\partial B_i}{\partial r} + \frac{\partial C_i}{\partial \theta} + D_i = 0 \tag{6}$$

The Lax technique can be extended to the problem which is being treated by replacing the partial derivative $\partial A_i/\partial t$ in equation (6) by the forward finite difference expression

$$\frac{1}{\Delta t}\left(\left(A_i\right)^{t+\Delta t}_{r,\theta} - \frac{1}{4}\left\{\left(A_i\right)^{t}_{r+\Delta r,\theta} + \left(A_i\right)^{t}_{r-\Delta r,\theta} + K\left[\left(A_i\right)^{t}_{r,\theta+\Delta\theta} + \left(A_i\right)^{t}_{r,\theta-\Delta\theta}\right]\right\}\right)$$

and substituting the central difference expressions

$$\frac{1}{2\Delta r}\left[\left(B_i\right)^{t}_{r+\Delta r,\theta} - \left(B_i\right)^{t}_{r-\Delta r,\theta}\right]$$

and

$$\frac{1}{2\Delta\theta}\left[\left(C_i\right)^t_{r,\theta+\Delta\theta} - \left(C_i\right)^t_{r,\theta-\Delta\theta}\right]$$

for the partial derivatives $\partial B_i/\partial r$ and $\partial C_i/\partial\theta$, respectively. The quantity K in the forward finite difference expression has the value $\sec\theta$ for the momentum equations (eqs. (2) and (3) above). For the continuity and energy equations (eqs. (1) and (4), respectively) K has a value of unity. This modification to the finite difference expressions for the time derivatives of the momentum equation is made in order that they will vanish for uniform flow parallel to the axis. The average value

$$\frac{1}{4}\left[\left(D_i\right)^t_{r+\Delta r,\theta} + \left(D_i\right)^t_{r-\Delta r,\theta} + \left(D_i\right)^t_{r,\theta+\Delta\theta} + \left(D_i\right)^t_{r,\theta-\Delta\theta}\right]$$

is used to represent the undifferentiated term in equation (6).

When these difference expressions are substituted into the partial differential equations and expanded about the point (r,θ,t), the following equation results:

$$\frac{\partial A_i}{\partial t} + \frac{\partial B_i}{\partial r} + \frac{\partial C_i}{\partial\theta} + D_i = -\frac{1}{2}\Delta t\frac{\partial^2 A_i}{\partial t^2} + \frac{1}{4}\frac{(\Delta r)^2}{\Delta t}\frac{\partial^2 A_i}{\partial r^2} + \frac{1}{4}\frac{(\Delta\theta)^2}{\Delta t}\frac{\partial^2 A_i}{\partial\theta^2} + O\left(\Delta^2\right) \quad (7)$$

This equation differs from the general form of the partial differential equations given by equation (6) because of the presence of the terms on the right-hand side. These terms cause the inviscid flow properties to be continuous across shock waves so that computations can be made in the vicinity of shocks in the same manner as elsewhere.

The procedure which is used in this investigation consists of using the forward time difference given above and another time difference given by

$$\frac{1}{\Delta t}\left\{\left(A_i\right)^{t+\Delta t}_{r,\theta} - \frac{1}{2}\left[\left(A_i\right)^{t}_{r+\Delta r,\theta} + \left(A_i\right)^{t}_{r-\Delta r,\theta}\right] + \frac{1}{8}\left[\left(A_i\right)^{t-\Delta t}_{r+2\Delta r,\theta} - 2\left(A_i\right)^{t-\Delta t}_{r,\theta} + \left(A_i\right)^{t-\Delta t}_{r-2\Delta r,\theta}\right]\right\}$$

on alternate time intervals. When the expansion for the first form of the time differences in equation (7) is replaced by that for the second form, the following equation results:

$$\frac{\partial A_i}{\partial t} + \frac{\partial B_i}{\partial r} + \frac{\partial C_i}{\partial \theta} + D_i = -\frac{1}{2}\Delta t \frac{\partial^2 A_i}{\partial t^2} + O\left(\Delta^2\right) \tag{8}$$

It has been found that the solutions which this alternating procedure yields are more accurate than those which are obtained when the first form of the time differences is used exclusively.

It has been shown that the Courant-Friedrichs-Lewy stability conditions are sufficient for both of the computational procedures mentioned above if allowance is made for the mixing of the flow properties in the vicinity of the smeared shocks.

RESULTS

Detailed Time-History Calculations

The diffraction of the incident shock wave by the sphere and the subsequent motion of the reflected shock wave for $\gamma = 1.4$ and $M_s = 5.55$ ($M_\infty = 1.70$) are shown in figures 1 and 2, where the Mach numbers M_s and M_∞ are those of the incident shock wave and the uniform flow behind the incident shock, respectively. The nondimensional time which is used is $\tau = ct/\delta_\infty$, where t is the time after shock impingement, c is the initial speed of the reflected shock, and δ_∞ is the steady shock detachment distance. The shock waves shown in the figures are positioned at the midpoints of the rapid rises

in the pressure profiles across the shocks. The computation is initiated at $\tau = -0.21$ before shock impingement has occurred. The shock wave moves downstream, strikes the sphere, and is reflected. Initially, the reflection is regular. When the angle of inclination of the incident shock to the surface has increased, Mach reflection occurs. Examples of regular and Mach reflection are shown in figure 1 for $\tau = 0.088$ and $\tau = 0.37$, respectively.

The movement of the reflected shock wave as steady flow is approached is shown in figure 2. The numerical results for the shock wave location at $\tau = 5.28$, and the experimental results of Ladenburg, Winckler, and Van Voorhis (9) are in agreement near the axis where the numerical solution has reached the steady state. The numerical solution is still slightly transient at points away from the axis and in the vicinity of the shock wave.

In figure 3, the transient stagnation streamline pressure distributions are shown. The pressure drops rapidly after the initial overpressure so that the pressure profile within the layer approaches its steady configuration before the shock detachment attains its steady value. The pressure profile at $\tau = 0.12$ shows the maximum value of the stagnation-point pressure that is encountered during the computation. It is seen in the figure that the maximum overpressure compares favorably with the pressure behind the reflected shock in the one-dimensional shock reflection problem. The time $\tau = 0$ corresponds to the time at which the incident shock should reach the body according to an exact one-dimensional shock computation. The numerically determined overpressure occurs a little later because the incident and reflected shock waves are smeared over several mesh spaces, and it takes several time steps for the reflection to occur.

6

The pressure distributions at $\tau = 5.28$ as determined by employing the two forms of the time differences alternately and by using the first form exclusively are compared in figure 3. The alternating procedure is seen to yield the best results. The stagnation-point thermodynamic properties are less in error, and the profiles are smeared less at the shock wave. It should be noted that the mesh spacings which are used for the two computations are identical; only the methods of computation differ.

Shock Detachment Distance Histories

Numerical results for the transient behavior of the shock detachment distance for several perfect-gas cases are presented in figure 4. The nondimensional quantity δ/δ_∞ is plotted against τ where the steady shock detachment distances δ_∞ are determined from the results of Van Dyke and Gordon (10) and Lomax and Inouye (11). The cases for $\gamma = 1.1$ and $\gamma = 1.4$ span a wide range of incident shock Mach number M_S. As M_∞ approaches unity the shock layer becomes large and difficult to compute when the steady state is approached. For this reason, the case $\gamma = 1.4$ and $M_S = 2.51$ $(M_\infty = 1.20)$ is terminated before steady flow is established. Since M_∞ is small for all values of M_S when γ is large, only one case is presented for $\gamma = 5/3$.

Results for two computations are shown in figure 4 for the case $\gamma = 1.1$ and $M_S = \infty$ $(M_\infty = 4.26)$. Finer mesh spacings are used for the computations indicated by the circles. The results show that the shock detachment histories are not very sensitive to the size of the mesh spacings.

All the curves in figure 11 lie in a fairly narrow band. This indicates that the nondimensional time τ is an effective scaling parameter. In general, the curves are arranged in ascending order within the band according to the value of M_∞.

Several cases are treated for $\gamma = 1.4$ to determine the asymptotic behavior of the shock detachment histories as M_s is increased. It is seen in figure 4 that the histories approach the limiting case for fairly low values of M_s; the curves for the cases $M_s = 30$ and $M_s = 3.7$ coincide for all means and purposes. In addition, the history of the shock detachment distance for the intermediate case $\gamma = 1.4$ and $M_s = 5.55$, the case which is illustrated in figures 1, 2, and 3, is represented by this curve.

Since the curves in figure 4 lie in a narrow band although γ varies over a wide range, it would appear that real-gas effects should not affect the shock detachment distance histories appreciably. Two cases for equilibrium air were treated to check this observation. These cases are illustrated in figure 5. It is seen that the curves for these cases lie within the band of perfect-gas solutions shown in figure 4.

A perfect-gas case is also shown in figure 5. The governing parameters γ and M_s for this case were chosen such that the Mach number M_∞ and the ratio of enthalpy to internal energy in the region of uniform flow behind the incident shock wave would match those of the equilibrium case where $U_s = 10,000$ fps, $p_o = 10^{-2}$ atmosphere, and $T_o = 32^\circ$ F. It is seen that the curves for the shock detachment distance histories for these cases coincide.

The equilibrium cases shown in figure 5 were computed with the aid of a curve fit of the thermodynamic properties. It can be seen from the governing differential equations, equations (1) to (4), that the finite difference equations determine the density ρ and the internal energy e at each new grid point. The curve fit is used to determine the pressure p and the enthalpy h in terms of ρ and e.

8

Stagnation-Point Pressure Histories

The numerical results for the stagnation-point pressure histories for several representative cases are presented in figure 6. The nondimensional pressure p_{stag}/p_∞ is plotted against τ. Initially, an overpressure occurs at the stagnation point. Then the pressure drops rapidly and approaches its steady value monotonically. The results of Butler (7) show that the transient stagnation-point pressure for a flat-nosed cylinder undershoots the steady value when γ is low and M_s is high. This phenomenon is not observed in the present results for the sphere. The maximum overpressures are in fair agreement with the pressures behind the reflected shocks for the one-dimensional shock reflection problems with similar values of M_s and γ. The numerical results for the steady stagnation-point pressures are in good agreement with the exact values.

The stagnation-point pressure histories for the perfect-gas case $M_s = 9.7$ and $\gamma = 1.24$ and the equilibrium-air case $U_s = 10,000$ fps, $p_0 = 10^{-2}$ atm, and $T_0 = 32^\circ$ F are compared in the figure. It is seen that these histories are similar.

A comparison of the results in figures 4 and 5 with those in figure 6 shows that the stagnation-point pressure approaches its steady value more rapidly than the shock detachment does. The pressures are within about 10 percent of the final values for $\tau = 1$. At this time, the shock detachment distances have reached only about 50 percent of their final values. The shock detachments approach their final values at $\tau = 5$ or 6. The asymptotic behavior of the other stagnation-point thermodynamic properties is similar to that of the pressure.

The mesh spacings $\Delta\theta$ and Δr are chosen such that $1^O \leqq \Delta\theta < 2^O$ and $\Delta r \leqq \delta_\infty/10$. It has been found that the shape of the curves for the stagnation point pressure histories is influenced by the mesh spacings. The waviness of these curves is reduced if the size of the mesh spacings is reduced.

Approximate Analytic Solution

A closed-form solution can be obtained for the shock detachment distance when M_∞ is large and γ is near unity. For these conditions, it can be assumed that the shock is concentric and the tangential velocity gradient varies linearly with distance behind the shock in the stagnation region. The density varies only slightly with position and time. The continuity equation is integrated across the shock layer using the one-strip method of integral relations. The time-dependent detachment distance is given by

$$\delta = \delta_\infty \left(1 - e^{-K\tau}\right) \left[1 - (1 - K)e^{-K\tau}\right]^{-1}$$

where

$$K = 1 - \rho_b \left[\left(\frac{dv}{d\theta}\right)_s - \left(\frac{dv}{d\theta}\right)_b\right] \left[\rho_b \left(\frac{dv}{d\theta}\right)_b + \rho_s \left(\frac{dv}{d\theta}\right)_s - \frac{3}{2}\rho_\infty U_\infty\right]^{-1}$$

The quantities subscripted with b and s are evaluated at the body and the shock, respectively, for steady flow.

The approximate solution for $\gamma = 1.1$ and $M_s = \infty$ is shown in figure 4.

CONCLUSIONS

It is shown that the transient flow about a sphere which has been washed by a normal shock wave is not coupled. The stagnation-point pressure adjusts

to the steady value more rapidly than the shock detachment distance. In addition, it is shown that the shock detachment distance histories of a number of perfect-gas cases can be scaled effectively.

REFERENCES

1. Cabannes, H.: Etude du Depart d'un Obstacle dans un Fluide au Repose. La Recherche Aeronautique, vol. 36, Nov.-Dec. 1953, pp. 7-12.

2. Bausset, Max: Etude du Depart d'un Obstacle dans un Fluide au Repose. C. R. Acad. Sc., Paris, vol. 261, Nov. 29, 1965, pp. 4613-4616.

3. Miles, J. W.; Mirels, H.; and Wang, H. E.: Time Required for Establishing Detached Bow Shock. AIAA J., vol. 4, no. 6, June 1966, pp. 1127-1128.

4. Davis, L.: Bow-Shock Establishment and Stagnation-Point Pressure Measurements for a Blunt-Nosed Body at Supersonic Speeds. NPL/AERO-1098, A.R.C.-25794, Hyp.-415, Aerodynamic Div., National Physics Laboratory, April 8, 1964.

5. Bryson, A. E.; and Gross, R. W. F.: Diffraction of Strong Shocks by Cones, Cylinders and Spheres. J. Fluid Mech., vol. 10, part 1, 1961, pp. 1-16.

6. Offenhartz, E.; and Weisblatt, H.: Determination of the Time History of the Flow about Blunt Bodies in a Shock Tube. Rep. Rad.-TR-2-58-4, Res. and Adv. Dev. Div., AVCO Manf. Corp., May 5, 1958.

7. Butler, T. D.: Numerical Calculations of the Transient Loading of Blunt Obstacles by Shocks in Air. AIAA J., vol. 4, no. 3, March 1966, pp. 460-467.

8. Lax, Peter D.: Weak Solutions of Nonlinear Hyperbolic Equations and Their Numerical Computation. Commun. Pure Appli. Math., vol. VII, no. 1, Feb. 1954, pp. 159-193.

9. Ladenburg, R.; Winckler, J.; and Van Voorhis, C. C.: Interferometric Studies of Faster than Sound Phenomena. Part I, The Gas Flow around Various Objects in a Free, Homogeneous, Supersonic Air Stream. Phys. Rev., vol. 73, no. 11, June 1948, pp. 1359-1377.

10. Van Dyke, Milton D.; and Gordon, Helen: Supersonic Flow Past a Family of
    Blunt Axisymmetric Bodies. NASA TR R-1, 1959.

11. Lomax, Howard; and Inouye, Mamoru: Numerical Analysis of Flow Properties
    about Blunt Bodies Moving at Supersonic Speeds in an Equilibrium Gas.
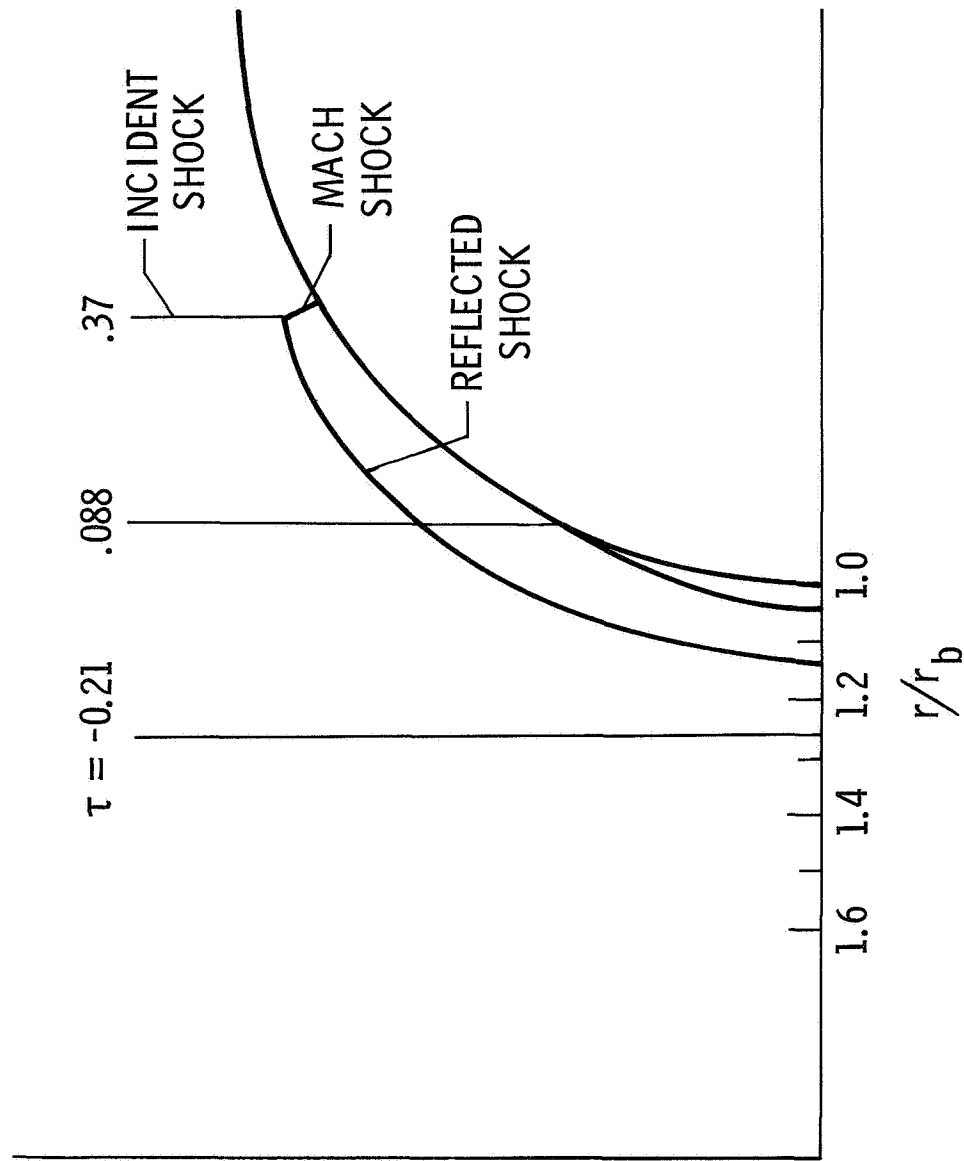   NASA TR R-207, July 1964.

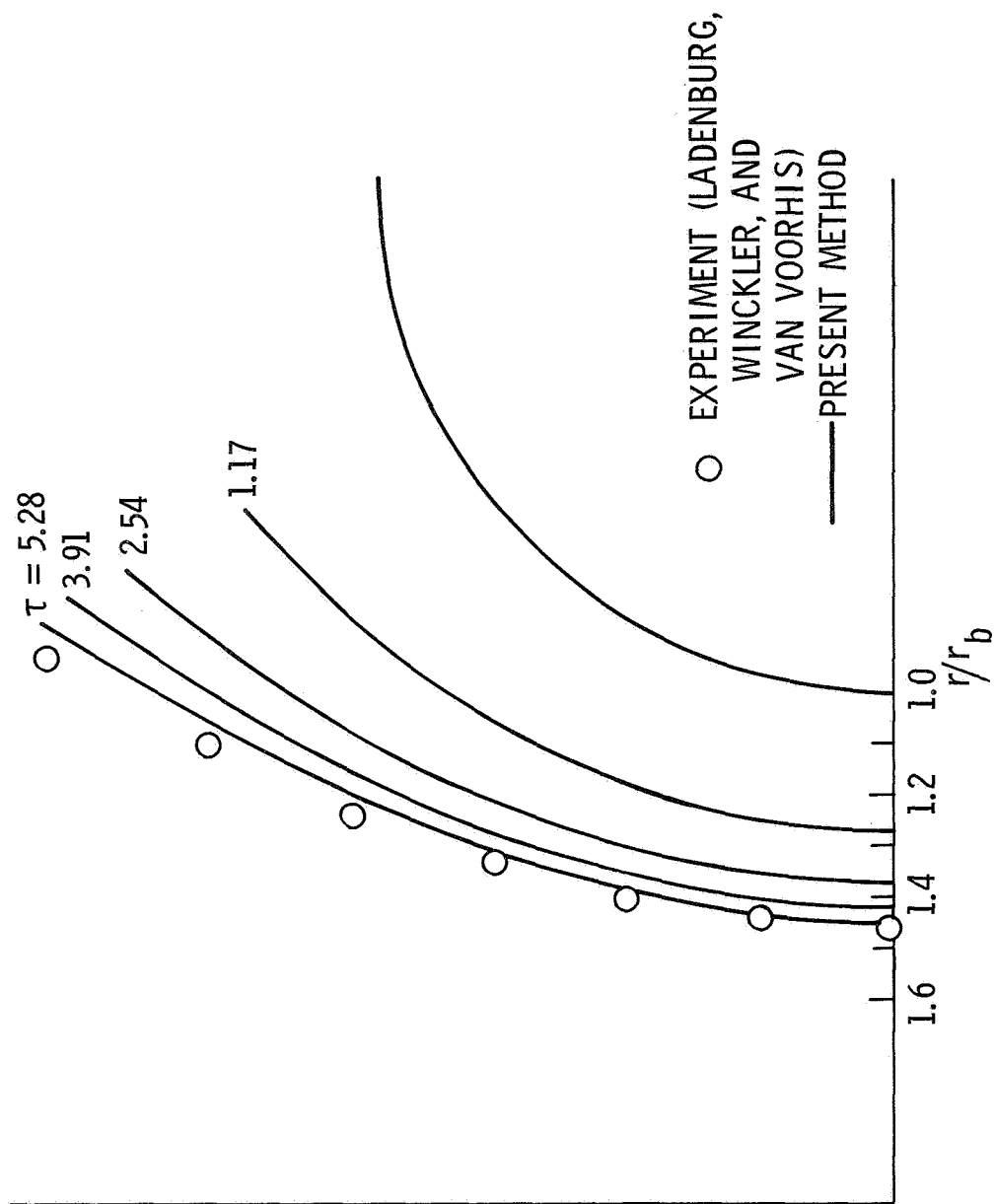Figure 1.- Normal shock wave-sphere interaction for $\gamma = 1.4$ and $M_s = 5.55$ ($M_\infty = 1.70$).
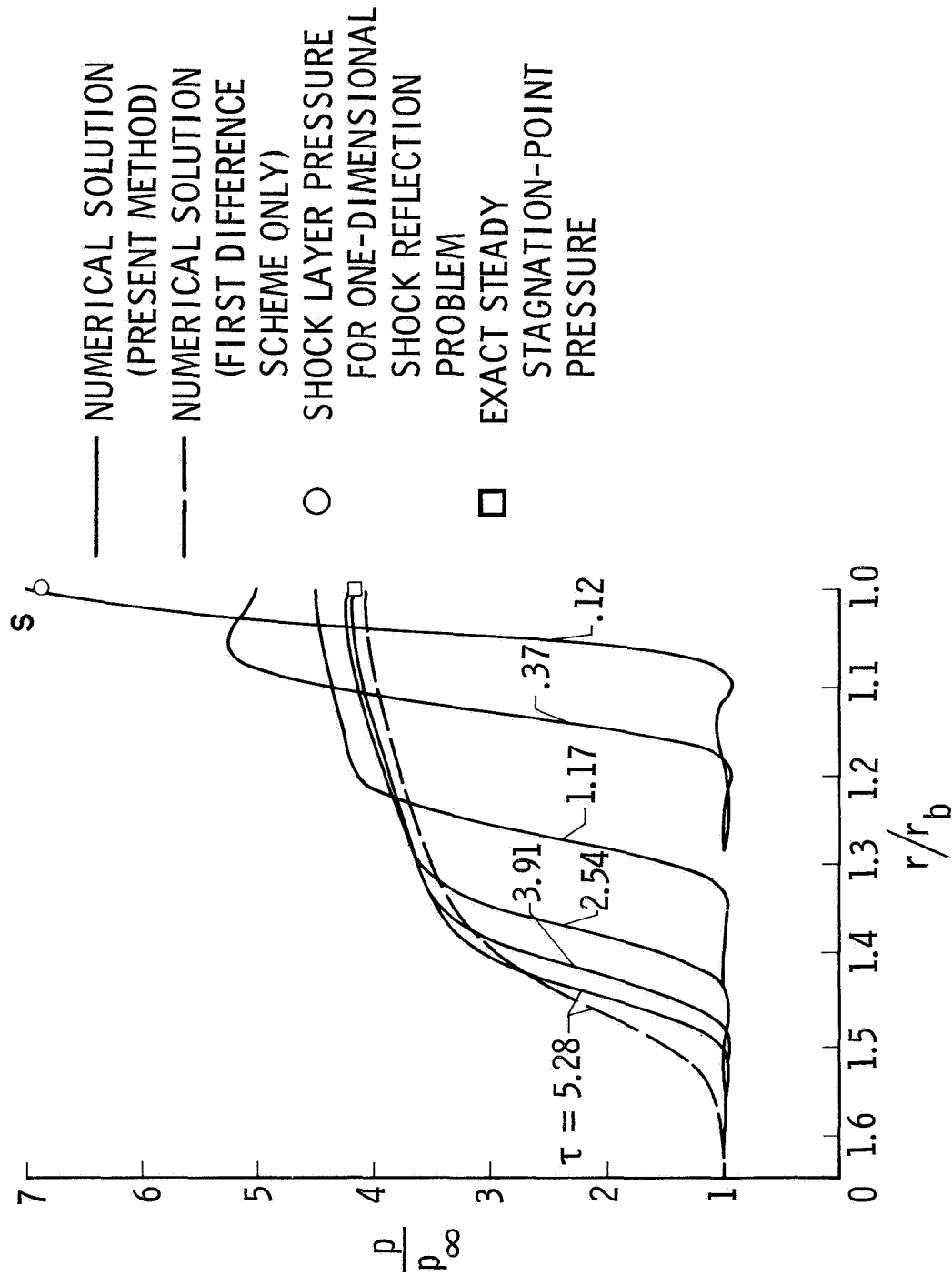
Figure 2.- Subsequent transient motion.

Figure 3.- Transient stagnation streamline pressure distributions for $\gamma = 1.4$ and $M_s = 5.55$ ($M_\infty = 1.70$).
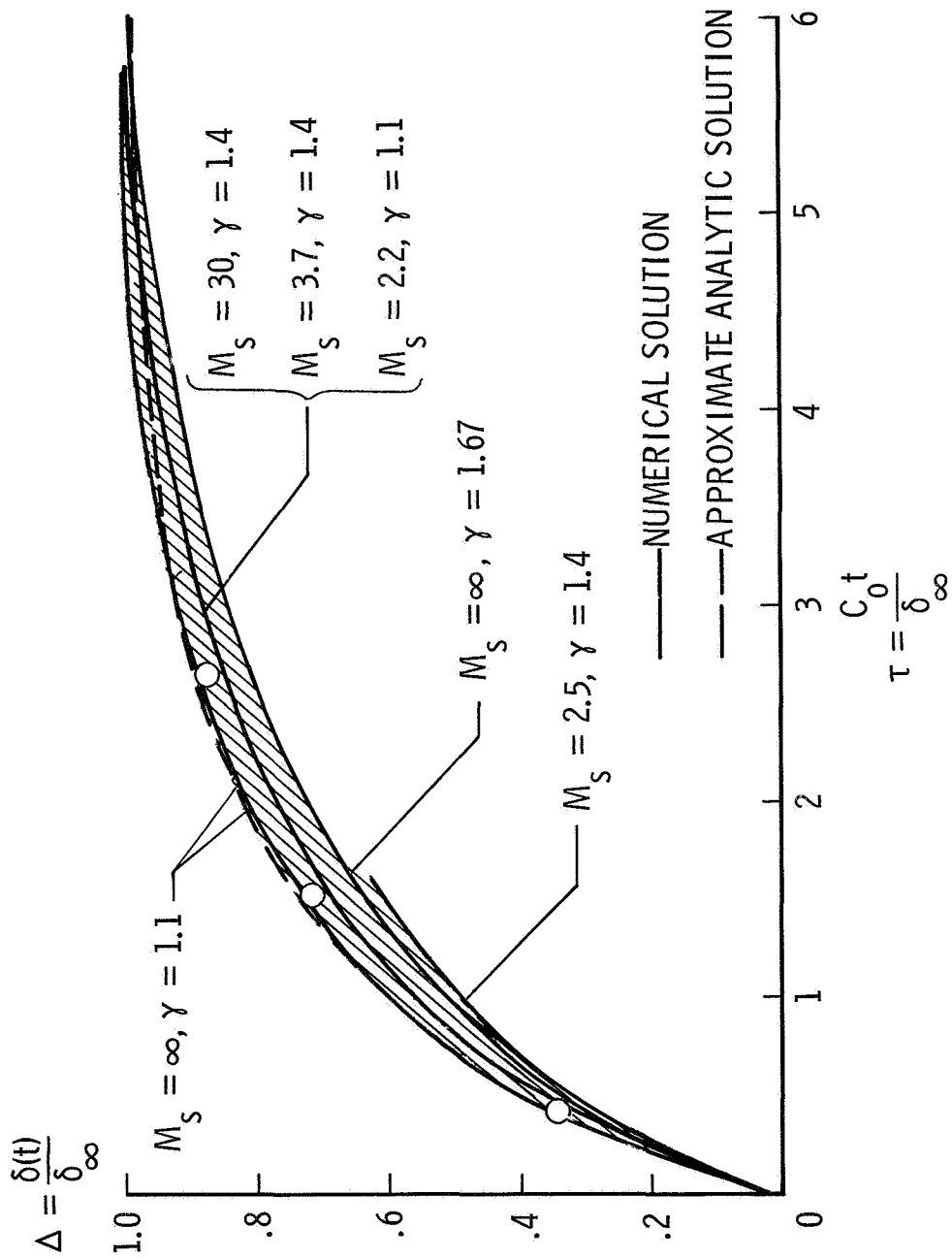
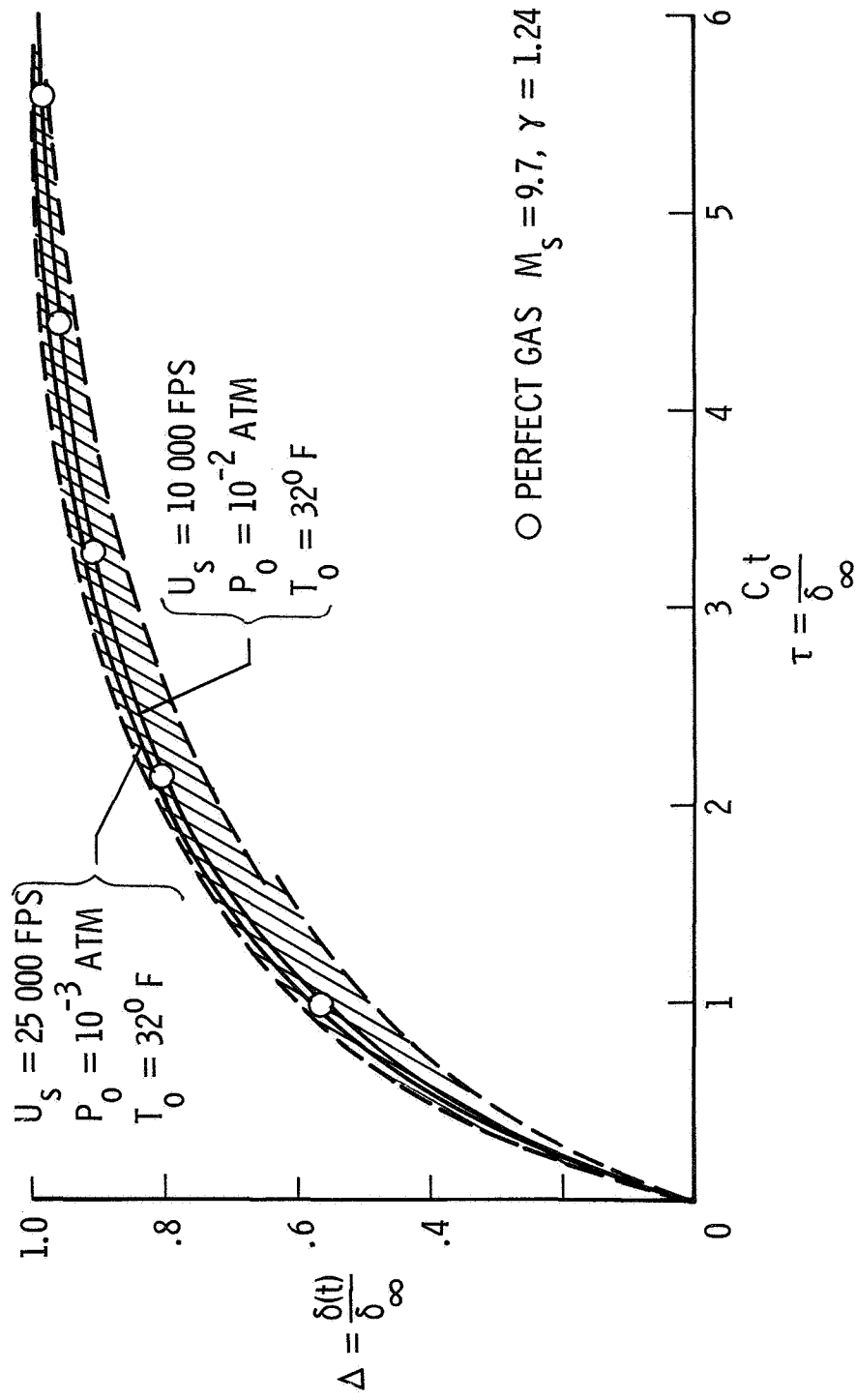Figure 4.- Perfect gas shock detachment distance histories.
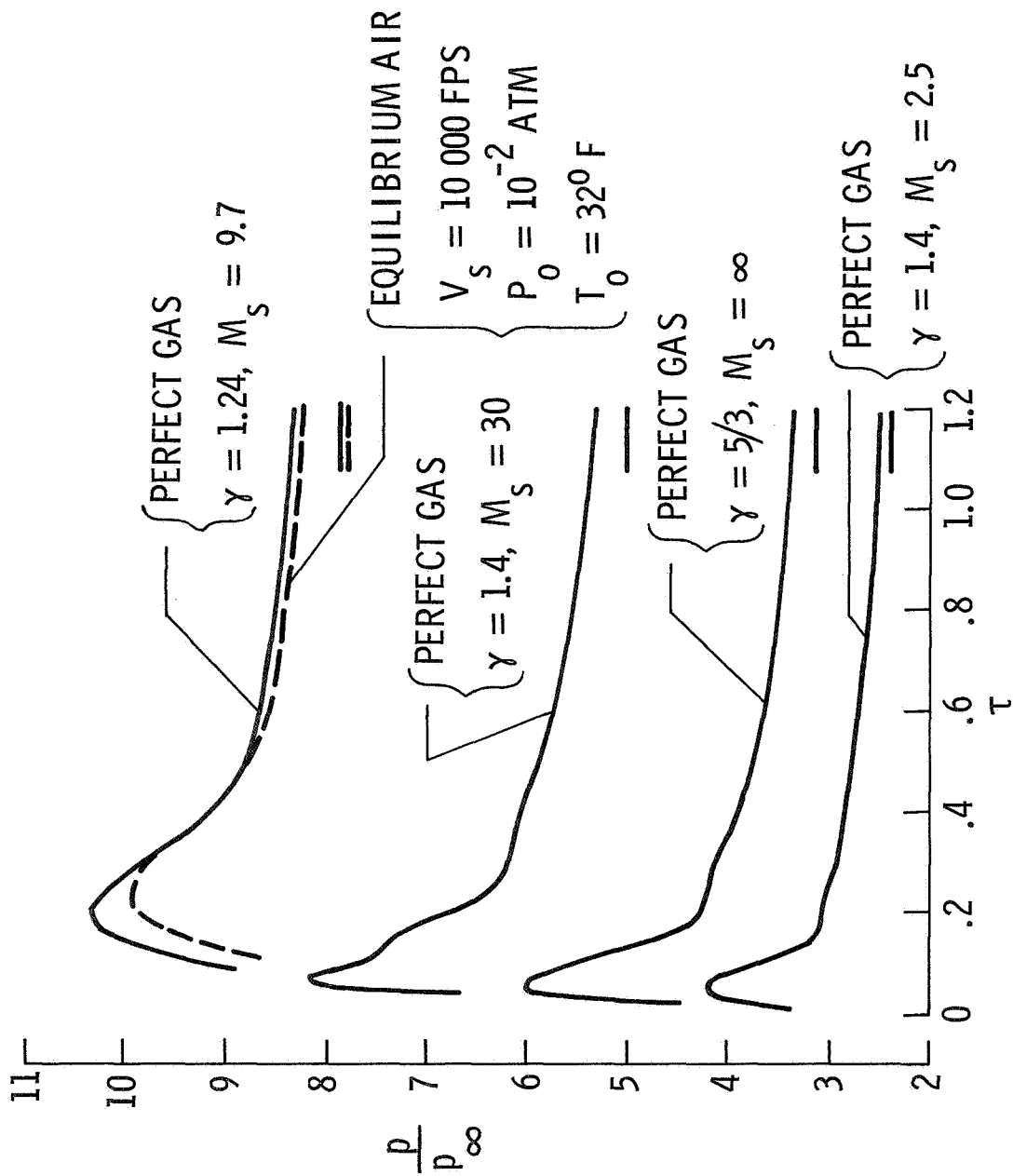
Figure 5.- Equilibrium air shock detachment distance histories.

Figure 6.- Stagnation point pressure histories.